

# Liquefaction of crushable granular media: a multiscale numerical analysis

Manuel Cárdenas-Barrantes<sup>1,2,\*</sup> and Carlos Ovalle<sup>1,2,\*\*</sup>

<sup>1</sup>Department of Civil, Geological and Mining Engineering, Polytechnique Montréal, Québec, Canada

<sup>2</sup>Institute for Research in Mines and the Environment (IRME) UQAT-Polytechnique, Québec, Canada

**Abstract.** Understanding liquefaction—the loss of shear resistance in granular materials under constant-volume shearing—is crucial for preventing landslides and geotechnical failures. This phenomenon typically occurs in water-saturated media during rapid undrained loading, such as seismic shocks. Liquefaction potential decreases with higher solid fraction and particle size polydispersity, but evolves if particle fragmentation occurs. We investigate the mechanics and microstructure of crushable, liquefiable granular materials through 2D undrained shear simulations. Results show that higher solid fractions and stronger particles delay liquefaction. Mechanical instabilities manifest as sharp drops in mean and deviatoric stresses, leading to resistance loss and fluid-like behavior. The redundancy number strongly correlates with shear resistance and contact network stability. At high solid fractions, grading upon fragmentation asymptotically approaches an ultimate state while maintaining stability. In contrast, looser samples exhibit earlier liquefaction, with fragmentation depending on particle strength. These findings highlight the critical role of particle strength in either mitigating or intensifying liquefaction.

## 1 Introduction

Understanding the mechanisms that trigger landslides is essential to improve prediction methods and mitigate their catastrophic impacts. Landslides can result from various mechanisms, such as liquefaction [1]. Liquefaction is defined as the loss of shear resistance in granular materials under undrained shearing, and is typically associated with loose granular soils. However, relatively dense samples could also liquefy if particle fragmentation occurs [2, 3], a phenomenon known as Sliding Surface Liquefaction (SSL) [4]. Some studies have proposed constitutive models to predict SSL-triggered failures [5, 6]. However, most of these models assume a continuous material response and do not explicitly capture particle-scale mechanisms.

To address particle-scale mechanisms, researchers have used the discrete element method (DEM) to study undrained shearing of crushable particles [7, 8], often using the particle replacement method [9] to simulate fragmentation. However, these studies focus mainly on triaxial shearing at relatively low strains and do not reach the liquefaction limit. Consequently, the micromechanics of SSL, including the role of particle strength and mean pressure, remain poorly understood. Furthermore, how fragmentation progresses towards an ultimate particle size distribution, as empirically observed [10, 11], and whether this sets a limit for liquefaction remains an open question.

This study presents a multiscale numerical analysis of SSL using the DEM and the bonded cell method. We con-

ducted virtual undrained shear tests on granular assemblies to investigate how microstructural evolution influences macroscopic liquefaction behavior. Specifically, we analyze the relationship between particle crushing, shear resistance, and the evolution of the particle size distribution toward the ultimate state.

## 2 Numerical Procedure

We performed 2D constant-volume shear numerical tests on granular configurations of crushable particles with varying particle strengths and granular densities. By imposing constant volume through periodic boundary conditions during the shear test, we emulate the undrained state of saturated soils under rapid loading, bypassing the need to simulate pore pressure and allowing us to compute effective stresses directly. The simulations were conducted using the DEM via the Contact Dynamics (CD) approach [12], implemented in the open-source software LMGC90 [13].

Each crushable particle was represented as a cell-based disk, generated by a centroidal Voronoi tessellation [14] using the software NEPER [15], with a fixed density of  $\rho_{cell} = \frac{88}{\pi d_{max}^2}$  [cells per unit area], where  $d_{max} = 1.0m$  is the diameter of the largest particle. To avoid ordering effects, the particle size polydispersity was set to  $d_{min}/d_{max} = 0.7$ , where  $d_{min}$  is the diameter of the smallest particle. The cells within each particle were bonded by normal cohesion  $\sigma_c$  (ranging from 0.2 to  $1.0 \cdot 10^4$  kPa), which represents particle strength [12, 16]. Bonds between cells break when local stress exceeds the normal cohesion and do not reform once broken.

\*e-mail: manuel.cardenas@polymtl.ca

\*\*e-mail: carlos.ovalle@polymtl.ca

Each sample contained  $2 \cdot 10^3$  particles (around  $20 \cdot 10^3$  cells). The particles were deposited layer by layer [17] in a square box of width and height  $36d_{max}$ . Uniaxial compression was applied in the vertical direction at a constant pressure  $P_0 = 10$  kPa with different friction coefficients, producing three different void ratios:  $e \in [0.212, 0.225, 0.235]$  (dense, medium-loose and loose, respectively), where  $e$  is defined as the ratio of the void area to the solid area. Periodic boundary conditions were imposed on the lateral borders so that particles reaching one side reappeared on the opposite side. Gravity was set to zero. Following the compaction, the friction coefficient was fixed at  $\mu = 0.4$  for all cases. A quasistatic shear test was then conducted by horizontally displacing the upper and lower walls at a constant velocity  $v_x = 5 \cdot 10^{-3} s^{-1} d_{max}$  while restricting their vertical displacements. To prevent strain localization at the boundaries, uncrushable particles were bonded to the upper and lower walls, introducing artificial roughness. Quasi-static conditions were ensured by maintaining the inertial number  $I = \dot{\gamma}d / \sqrt{P_0/\rho}$  below  $10^{-4}$ , with the shear rate  $\dot{\gamma} = v_x/h = 1.4 \cdot 10^{-4} s^{-1}$ ,  $d$  the mean particle diameter, and  $\rho = 2.7 \cdot 10^3$  kg  $m^{-2}$  the particle density [18]. Further details on the numerical approach can be found in [19].

### 3 Macromechanics

Constant volume shearing conditions in granular soils limit macroscopic dilation and contraction, requiring internal structural reorganization. This leads to significant microstructural changes and variations in effective stress, which increase in dense media but potentially decrease drastically in loose ones (liquefaction). In addition, shearing stresses can induce particle fragmentation, further promoting contraction and reducing effective stress. Figure 1 shows two strain stages and their corresponding levels of fragmentation for a dense sample ( $e = 0.212$ ).

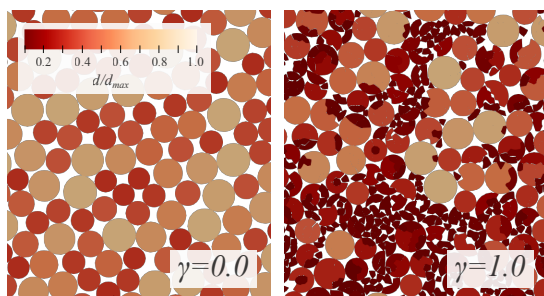


**Figure 1.** Two strain stages ( $\gamma = 0.0$  and  $1.0$ , respectively) for  $e = 0.212$  and  $\sigma_c = 1.0 \cdot 10^3 P_0$ . Colors, ranging from dark blue to light blue, represent particle sizes scaled by  $d_{max}$ .

Figures 2(a) and (b) show the mean stress behavior ( $p'$ ) and the deviatoric ( $q$ ) stress-strain behavior for the three densities studied and different particle strengths. Particle fragmentation causes substantial stress variations across all samples. However, all exhibit initial hardening (i.e., increasing  $q$  and  $p'$ ) over a small strain range, with peak values proportional to the density and the particle strength. This is followed by strain softening at large

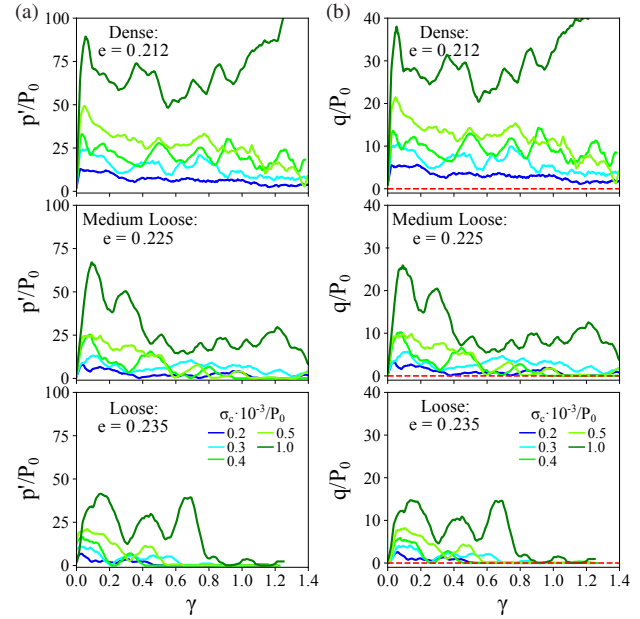


**Figure 2.** (a)  $p'/P_0$  and (b)  $q/P_0$  as a function of  $\gamma$ . The dashed red line signals  $q = 0$ .

strain, except for the dense case with the strongest particles ( $\sigma_c = 1.0 \cdot 10^3 P_0$ ), which undergoes limited softening until  $\gamma = 0.6$  and, then, significant hardening due to a dilatant-like increase in effective stress. Defining liquefaction as the complete loss of macromechanical shear resistance (i.e.,  $q = 0$ ), none of the dense samples with strain softening liquefied. In contrast, all loose samples liquefied, regardless of particle strength, while only one medium-loose sample did not. This sample exhibited a peak  $q/P_0 \approx 20$  and softened to  $q/P_0 \approx 10$ , similar to the dense case at  $\sigma_c = 0.5 \cdot 10^3 P_0$ .

The observed reduction in shear and stress resistance with decreasing density is linked to the evolution of the particle shape after fragmentation. Greater crushing in denser samples produces more angular fragments (Figure 1), enhancing macromechanical resistance [20, 21].

### 4 Redundancy number

A way to measure the packing connectivity and clearly assess the stability of the contact network is through the redundancy number  $i_r$  [22], making it an excellent indicator for evaluating liquefaction.  $i_r$  is the ratio between the number of constraints and the system's degrees of freedom, defined as:

$$i_r = \frac{N_c \left(2 - \frac{N_s}{N_c}\right)}{3N \left(1 - \frac{N_r}{N}\right)}, \quad (1)$$

where  $N_c$  is the total number of contacts,  $N_s$  is the number of sliding contacts,  $N$  is the number of particles, and  $N_r$  is the number of rattlers (particles with zero or one contact). Theoretically, a sample reaches stability when the number of constraints equals the number of degrees of freedom in the system; i.e., the isostatic state,  $i_r = 1$ . In hyperstatic

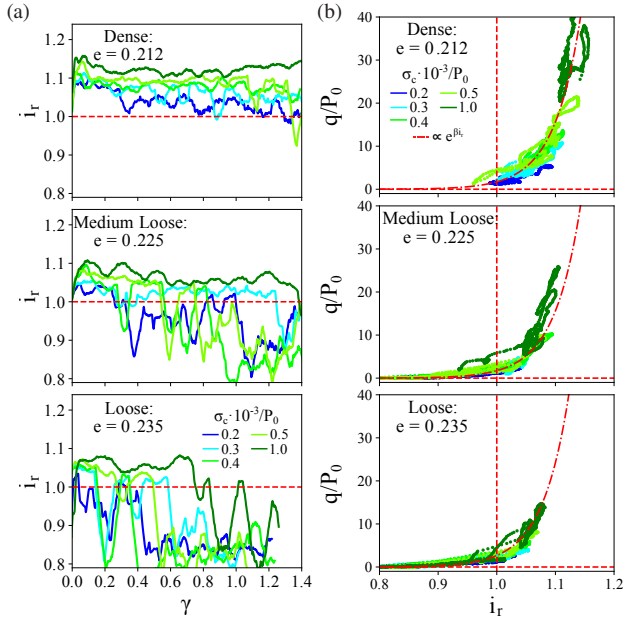


**Figure 3.** (a)  $i_r$  as a function of  $\gamma$ . The horizontal dashed red line indicates  $i_r = 1$ . (b)  $q/P_0$  as a function of  $i_r$ . The horizontal and vertical dashed red lines signals  $q = 0$  and  $i_r = 1$ . The red dashed-dotted line shows an exponential fit of the trend across all cases.

states ( $i_r > 1$ ), the system is mechanically stable and exhibits solid-like behavior, allowing the load during shear to be redistributed more effectively through multiple contacts and pathways. In contrast, in under-static states ( $i_r < 1$ ), the number of constraints is insufficient to fully restrict the degrees of freedom of the particles, making the system mechanically unstable. A reduced number of constraints, reflected in a reduced number of contacts, limits the possible load redistribution pathways during shear, creating instabilities. These instabilities can eventually propagate and culminate in liquefaction, leading to system collapse. Figure 3(a) shows the variation of  $i_r$  with  $\gamma$ . A decrease in  $i_r$  is observed as the particle strength decreases, with a greater and faster decline occurring in lower-density samples. This corroborates the earlier sharp drop in mean and deviatoric stresses, confirming that these states effectively correspond to liquefaction.

To compare the structural stability with the macro-mechanical resistance, Figure 3(b) presents the relationship between  $i_r$  and  $q$ . Interestingly, while all three densities studied eventually reach states with  $i_r < 1.0$ , not all of these states lead to liquefaction. In other words, a redundancy number below 1 does not necessarily indicate zero shear resistance. Instead, liquefaction is observed for  $i_r < 0.9$ . Furthermore, a higher particle strength contributes to a greater shear resistance and, consequently, higher redundancy numbers. A master curve reveals an exponential relationship between resistance and redundancy,  $q \propto e^{\beta i_r}$ , across all cases (red dashed-dotted line in Figure 3(b)). Our simulations give  $\beta = 22 \pm 3$ , suggesting that, regardless of  $e$  and  $\sigma_c$ , the decrease in  $q$  relative to the  $i_r$  follows a quasi-unique path.

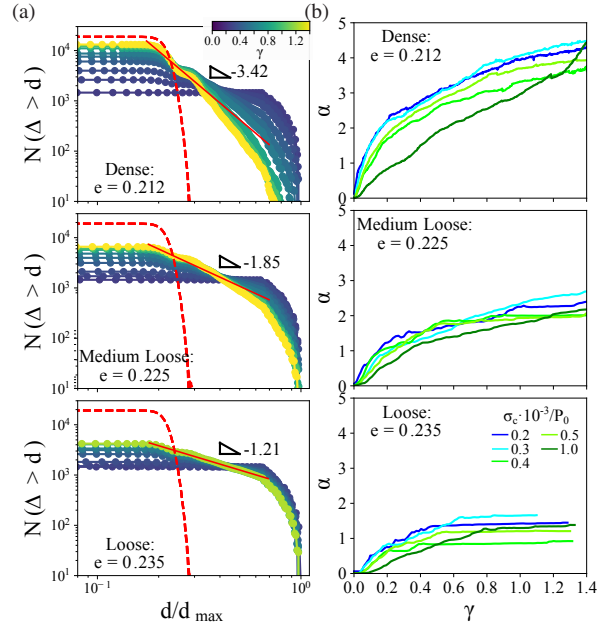


**Figure 4.** (a) particle size distributions as a function of  $\gamma$  for a sample with  $\sigma_c = 0.5 \cdot 10^3 P_0$ . (b) Evolution of  $\alpha$  as a function of  $\gamma$  for all studied samples. The red dashed line shows the numerical distribution limit. The solid red line shows the power-law fit of the UFS.

## 5 Grading evolution

The process of particle crushing significantly influences the liquefaction potential by continuously altering the size and shape of the crushed fragments. Figure 4(a) illustrates this transformation, showing the particle size distributions as a function of  $\gamma$  for a granular strength of  $\sigma_c = 0.5 \cdot 10^3 P_0$ . The particle size is defined by an effective diameter derived from the particle area, as their shapes are no longer circular after fragmentation. Initially, the particles have a uniform size distribution, ranging between  $d_{max}$  and  $d_{min}$ . As shearing progresses, the particle size distribution asymptotically evolves toward an Ultimate Fragmentation State (UFS) that depends on  $e$ . This transition occurs earlier than the numerical crushed limit (red dashed lines in Figure 4(a)). Medium-loose and loose samples show a slower progression toward the UFS, suggesting that they experience less fragmentation under the same strain levels. In simulations and experiments on the compaction of crushable materials, the size distribution of the UFS follows a power-law form with an exponent  $\alpha$  ( $N \propto d^{-\alpha}$ ), which is characteristic of fractal behavior [11]. In our case, under constant volume conditions, the UFS exhibits the same power law behavior (see the solid red line in Figure 4(a)). Figure 4(b) shows the asymptotic evolution of  $\alpha$  as a function of  $\gamma$ . Both the evolution of  $\alpha$  and its asymptotic value appear to be more sensitive to the density of the system than to the strength of the particles, corroborating that  $\alpha$  is a general geometric parameter. A dense system has limited possibilities for reorganization and is therefore more susceptible to grain fragmentation, with particle strength primarily determining the rate at which the UFS is reached. In contrast, a loose system

has more room for reorganization, leading to lower values of  $\alpha$ .

## 6 Conclusions

We study Sliding Surface Liquefaction (SSL) using 2D virtual tests with the Contact Dynamics (CD) method, examining dense, medium-loose, and loose assemblies. In the densest sample with the strongest particles, we observed dilative behavior, where effective stresses increased at high strains. Lowering particle strength or density led to strain softening. In all loose samples and medium-loose samples with weaker particles, this resulted in liquefaction, marked by a complete loss of shear resistance. Regardless of particle strength, the grain size distribution always approaches an ultimate state at large shear strains that depends on the granular density. Since dense samples generally experience more particle crushing than loose ones, the extent of fragmentation does not directly correlate with the occurrence of liquefaction. Future studies could explore 3D systems, where particles may rearrange differently and show more contraction after crushing due to extra movement possibilities. Adding more realistic shapes and breakage models could also help capture natural grain behavior. Still, our 2D results reflect key physical processes that should also appear in 3D.

## References

- [1] K. Ishihara, *Soil Behaviour in Earthquake Geotechnics* (Clarendon Press, London, 1996)
- [2] M. Hyodo, Y. Wu, N. Aramaki, Y. Nakata, Undrained monotonic and cyclic shear response and particle crushing of silica sand at low and high pressures, *Can. Geotech. J.* **54**, 207 (2017). [10.1139/cgj-2016-0212](https://doi.org/10.1139/cgj-2016-0212)
- [3] K. Sassa, H. Fukuoka, G. Wang, N. Ishikawa, Undrained dynamic-loading ring-shear apparatus and its application to landslide dynamics, *Landslides* **1**, 7 (2004). [10.1007/s10346-003-0004-y](https://doi.org/10.1007/s10346-003-0004-y)
- [4] K. Sassa, H. Fukuoka, G. Scarascia-Mugnozza, S. Evans, Earthquake-induced-landslides: Distribution, motion and mechanisms, *Soils Found.* **36**, 53 (1996). [10.3208/sandf.36.Special\\_53](https://doi.org/10.3208/sandf.36.Special_53)
- [5] N. Gerolymos, G. Gazetas, A model for grain-crushing-induced landslides—application to nikawa, kobe 1995, *Soil Dyn. Earthq. Eng.* **27**, 803 (2007). [10.1016/j.soildyn.2007.01.003](https://doi.org/10.1016/j.soildyn.2007.01.003)
- [6] Z. Chen, S. He, Simulation of effects of particle breakage on sliding surface friction for a hypothetical soil continuum moving on an inclined plane, *Landslides* **17**, 2113 (2020). [10.1007/s10346-020-01404-8](https://doi.org/10.1007/s10346-020-01404-8)
- [7] J.P. de Bono, G.R. McDowell, Micro mechanics of drained and undrained shearing of compacted and overconsolidated crushable sand, *Géotechnique* **68**, 575 (2018). [10.1680/jgeot.16.P.318](https://doi.org/10.1680/jgeot.16.P.318)
- [8] D. Shi, D. Cao, J. Xue, Y. Deng, Y. Liang, Dem studies on the effect of particle breakage on the critical state behaviours of granular soils under undrained shear conditions, *Acta Geotech.* **17**, 4865 (2022). [10.1007/s11440-022-01580-y](https://doi.org/10.1007/s11440-022-01580-y)
- [9] J.A. Åström, H.J. Herrmann, Fragmentation of grains in a two-dimensional packing, *EPJ B* **5**, 551 (1998). [10.1007/s100510050476](https://doi.org/10.1007/s100510050476)
- [10] M.R. Coop, K.K. Sorensen, T. Bodas Freitas, G. Georgoutsos, Particle breakage during shearing of a carbonate sand, *Géotechnique* **54**, 157 (2004). [10.1680/geot.2004.54.3.157](https://doi.org/10.1680/geot.2004.54.3.157)
- [11] D.L. Turcotte, Fractals and fragmentation, *J. Geophys. Res. Solid Earth.* **91**, 1921 (1986). [10.1029/JB091iB02p01921](https://doi.org/10.1029/JB091iB02p01921)
- [12] F. Radjai, Contact dynamics method, *Eur. J. Environ. Civ. En.* **12**, 871 (2008). [10.1080/19648189.2008.9693052](https://doi.org/10.1080/19648189.2008.9693052)
- [13] F. Dubois, M. Jean, M. Renouf, R. Mozul, A. Martin, M. Bagneris, Lmgc90, in *10e colloque national en calcul des structures* (2011), pp. Clé–USB
- [14] Q. Du, V. Faber, M. Gunzburger, Centroidal voronoi tessellations: Applications and algorithms, *SIREV* **41**, 637 (1999). [10.1137/S0036144599352836](https://doi.org/10.1137/S0036144599352836)
- [15] R. Quey, P. Dawson, F. Barbe, Large-scale 3d random polycrystals for the finite element method: Generation, meshing and remeshing, *Comput. Methods Appl. Mech. Eng.* **200**, 1729 (2011). [10.1016/j.cma.2011.01.002](https://doi.org/10.1016/j.cma.2011.01.002)
- [16] Y. Huilca, M. Silva, C. Ovalle, J.C. Quezada, S. Carrasco, G.E. Villavicencio, Modelling size effect on rock aggregates strength using a dem bonded-cell model, *Acta Geotech.* **16**, 699 (2021). [10.1007/s11440-020-01054-z](https://doi.org/10.1007/s11440-020-01054-z)
- [17] C. Voivret, F. Radjai, J.Y. Delenne, M.S. El Yousoufi, Space-filling properties of polydisperse granular media, *Phys. Rev. E* **76**, 021301 (2007). [10.1103/PhysRevE.76.021301](https://doi.org/10.1103/PhysRevE.76.021301)
- [18] Y.F. Bruno Andeotti, O. Pouliquen, *GRANULAR MEDIA, Between Fluid and Solid* (Cambridge University Press, London, 2013)
- [19] M. Cárdenas-Barrantes, C. Ovalle, Multiscale insights into sliding surface liquefaction through dem simulations, *Comput. Geotech.* **183**, 107191 (2025). [10.1016/j.compgeo.2025.107191](https://doi.org/10.1016/j.compgeo.2025.107191)
- [20] S. Carrasco, D. Cantor, C. Ovalle, F. Dubois, Particle shape distribution effects on the critical strength of granular materials, *Comput. Geotech.* **177**, 106896 (2025). [10.1016/j.compgeo.2024.106896](https://doi.org/10.1016/j.compgeo.2024.106896)
- [21] C. Ovalle, C. Dano, Effects of particle size–strength and size–shape correlations on parallel grading scaling, *Géotechnique Lett.* **10**, 191 (2020). [10.1680/jgele.19.00095](https://doi.org/10.1680/jgele.19.00095)
- [22] M. Pouragha, R. Wan, Onset of structural evolution in granular materials as a redundancy problem, *Granul. Matter* **18**, 38 (2016). [10.1007/s10035-016-0640-2](https://doi.org/10.1007/s10035-016-0640-2)